ELSEVIER

Image and Vision Computing 17 (1999) 201–212

image AND vision COMPUTING

Coherence-enhancing diffusion of colour images ☆

Joachim Weickert*

Department of Computer Science, University of Copenhagen, Universitetsparken 1, DK-2100 Copenhagen, Denmark

Received 1 August 1997; received in revised form 11 March 1998; accepted 12 March 1998

Abstract

Many image processing problems require the enhancement of coherent flow-like structures. This can be accomplished in a natural way by combining anisotropic diffusion filtering and texture analysis by means of the structure tensor (second-moment matrix, interest operator). In this paper an extension of these ideas to vector-valued images is presented. A structure tensor for vector-valued images is constructed as the mean of the structure tensors of each channel. This idea generalizes Di Zenzo's gradient for colour images by introducing an additional integration scale. The common structure tensor is used for steering the diffusion processes in each channel. The additional integration scale turns out to be crucial for orientation smoothing and it leads to significantly improved filter results. After analysing the role of all filter parameters, examples from different application areas are presented, and it is demonstrated that this type of diffusion filtering is highly robust under additive Gaussian noise.

Keywords: Image processing; Flow-like structures; Structure tensor; Nonlinear diffusion; Scale-space; Vector-valued images

1. Introduction

Flow-like structures appear in many image processing problems, for instance the automatic assessment of wood surfaces or fabrics, fingerprint analysis, or scientific image processing in oceanography [1]. Most humans consider flow-like structures as pleasant, harmonic, or at least interesting. Thus, it is not surprising that also artists like van Gogh or Munch have emphasized these features in their paintings.

Some images containing flow-like patterns are of poor quality, such that it becomes necessary to enhance them by closing interrupted lines[1]. Moreover, in many 'natural' images, colour plays an important role and it would be desirable to make use of this additional information. Vector-valued image processing material with coherent structures, however, can also arise in meteorology and oceanography, if information is collected at different channels corresponding to different wavelengths.

In the present paper we shall address the problem of enhancing such flow-like structures in vector-valued images. To this end, we first have to *analyse* their coherence. This is done by generalizing a well-established tool from texture analysis, the structure tensor (second-moment matrix, interest operator) to vector-valued images. Its eigenvectors and eigenvalues provide us with all required information. This coherence descriptor enables us to construct a diffusion tensor which steers the diffusion process in each channel in such a way that diffusion is encouraged along the preferred structure orientation.

The paper is organized as follows. Section 2 gives a review of the structure tensor concept and it presents its generalization to vector-valued images. Then we discuss in Section 3 how this information is used for designing an appropriate diffusion process. Its parameters are analysed in Section 4, and its properties are illustrated by several examples in Section 5. We conclude with a summary in Section 6.

1.1. Related work

The work presented here makes a synthesis of two earlier ideas of the author: Using a common structure tensor for diffusing vector-valued images was proposed in [2], while scalar-valued coherence-enhancing anisotropic diffusion goes back to [3]. Its distinctive feature is the combination of colour texture processing based on structure tensor analysis with a nonvanishing integration scale.

This concept also generalizes work of Whitaker and Gerig [4] for isotropic diffusion of vector-valued images

* Tel: +45 35321359; fax: +45 35321401; e-mail: joachim@diku.dk

☆ Extended version of a presentation at the Seventh National Symposium on Pattern Recognition and Image Analysis (Barcelona, April 21–25, 1997).

[1] This problem can even be related to finding illusory contours.

0262-8856/99/$ - see front matter
PII: S0262-8856(98)00102-4

with a common scalar diffusivity to the anisotropic case with a common diffusion tensor. Recently, different techniques which are based on partial differential equations (PDEs) have been applied to colour images [5–10]. Among them, the ones by Chambolle [6] and Sapiro and Ringach [9] reveal the most structural similarities to our approach. However, their goal is edge-preserving smoothing, while the method presented here achieves coherence-enhancement by looking at an additional, much larger scale: the integration scale. We shall see that this is a very essential model feature which guarantees stable orientation estimates. This additional integration scale is also the main difference to the anisotropic diffusion approach of Cottet and Germain [11] for scalar images.

Related anisotropic techniques which convolve with a Gaussian, whose shape is adapted to a second moment matrix, have been pioneered by Nitzberg and Shiota [12], and further pursued by Lindeberg and Gårding [13] and Yang et al. [14]. Unlike our approach they do not utilize the difference of the eigenvalues of the structure tensor as a coherence measure, and they focus on scalar images. In this sense they are more similar to the methods presented in [15], but they are not equivalent to a diffusion process in divergence form, which is capable of preserving the average grey value.

PDE methods for texture smoothing or enhancement often create a feature vector image by means of Gabor techniques, apply a nonlinear vector-valued diffusion to this feature image, and assemble the filtered texture from the processed features. Techniques in this spirit have been proposed by Whitaker and Gerig [4], Rubner and Tomasi [16], and Kimmel et al. [7]. Although these methods make use of generalized gradients for vector-valued images in the sense of Kreyzsig [18] and Di Zenzo [19], they do not take into account the integration scale. Recently, a PDE-based smoothing method which utilizes Gabor filters and which works directly on the image (instead of the feature vector image) has been studied by Carmona and Zhong [17]. Most of the preceding texture processing methods were designed for grey-scale images, and techniques such as [7,16,17] do not necessarily lead to diffusion processes in divergence form.

Since our method works on colour textures and may serve to create visually more pleasant structures with increased coherence, it is not surprising that it gives perceptually similar results as the line integral convolution method by Cabral and Leedom [20], which has become a popular tool

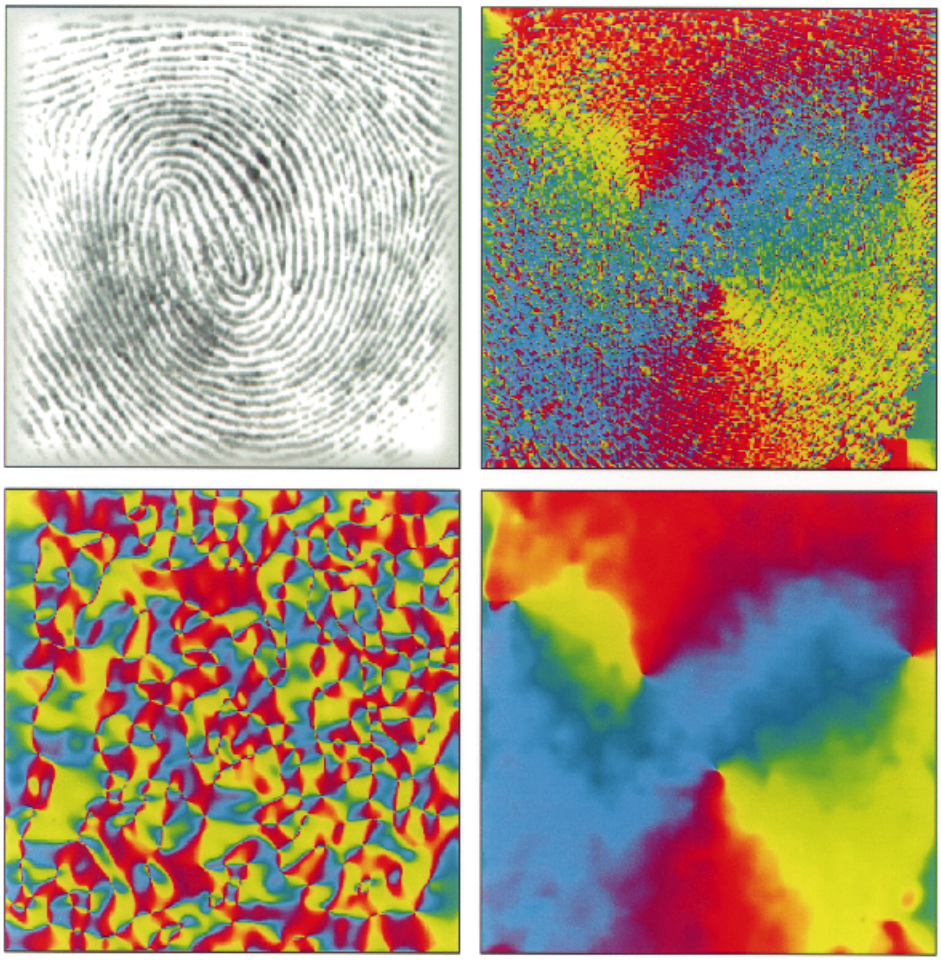

Fig. 1. Local orientation in a fingerprint image. (a) Top left: Original fingerprint, $\Omega = (0,256)^2$. (b) Top right: Orientation of smoothed gradient, $\sigma = 0.5$. (c) Bottom left: Orientation of smoothed gradient, $\sigma = 5$. (d) Bottom right: Structure tensor orientation, $\sigma = 0.5$, $\rho = 4$. Adapted from [3].

in computer graphics. A preliminary version of the present paper can be found in a proceedings volume [21].

2. Analysing coherent structures

For analysing coherent flow-like structures, we first focus on scalar images. Consider a rectangular image domain $\Omega := (0,a_1) \times (0,a_2)$, and let an image $u(x)$ be represented by a bounded mapping $u:\Omega \to \mathbb{R}$.

A very simple structure descriptor is given by ∇u_σ, the gradient of a Gaussian-smoothed version of u:

$$K_\sigma(x) := \frac{1}{2\pi\sigma^2} \cdot \exp\left(-\frac{|x|^2}{2\sigma^2}\right) \tag{1}$$

$$u_\sigma(x,t) := (K_\sigma * u(.,t))(x) \quad (\sigma > 0) \tag{2}$$

The standard deviation σ denotes the *noise scale,* since it makes the edge detector ignorant of details smaller than $O(\sigma)$. Although ∇u_σ is useful for detecting edges, it is unsuited for finding parallel structures, as we can see from Fig. 1. The left image shows an original fingerprint. Fig. 1(b,c) depicts the gradient orientation using colours: vertical gradients are depicted in red, horizontal ones in green, etc. We observe that for small σ, high fluctuations remain, while larger σ lead to entirely useless results. This is due to the fact that for larger σ neighbouring gradients with the same orientation, but opposite sign cancel each other. Gradient smoothing averages directions instead of orientations[2]. To make the structure descriptor invariant under sign changes, we may replace ∇u_σ, by its tensor product

$$J_0(\nabla u_\sigma) := \nabla u_\sigma \nabla u_\sigma^T \tag{3}$$

This matrix is symmetric and positive semidefinite, and its eigenvectors are parallel and orthogonal to ∇u_σ, respectively. The corresponding eigenvalues $|\nabla u_\sigma|^2$ and 0 describe the contrast in the eigendirections. Now that we have replaced directions by orientations, we can average the orientations by applying a componentwise convolution with a Gaussian K_ρ:

$$J_\rho(\nabla u_\sigma) := K_\rho * (\nabla u_\sigma \nabla u_\sigma^T) \quad (\rho \geq 0) \tag{4}$$

This matrix is named *structure tensor, interest operator* or *second-moment matrix*. It is useful for many different tasks, for instance for analysing flow-like textures [22], corners and *T*-junctions [12,23,24], shape cues [25] and spatiotemporal image sequences [1]. Equivalent approaches may also be found in [26,27]. A book by Jähne [1] gives a nice overview of these methods and clarifies their equivalence.

It is not hard to verify that the symmetric matrix

$$J_\rho = \begin{pmatrix} j_{11} & j_{12} \\ j_{12} & j_{22} \end{pmatrix}$$

is positive semidefinite. Its eigenvalues can be calculated as

$$\mu_{1,2} = \frac{1}{2}\left(\text{trace}(J_\rho) \pm \sqrt{\text{trace}^2(J_\rho) - 4\det(J_\rho)}\right) \tag{5}$$

where $\text{trace}(J_\rho) = j_{11} + j_{22}$, $\det(J_\rho) = j_{11}j_{22} - j_{12}^2$, and $\mu_1 \geq \mu_2$. The corresponding orthonormal set of eigenvectors $\{w_1,w_2\}$ is given by $w_1 = (\cos\phi, \sin\phi)^T$, where ϕ satisfies

$$\tan(2\phi) = \frac{2j_{12}}{j_{11} - j_{22}} \tag{6}$$

The eigenvalues integrate the variation of the grey values within a neighbourhood of size $O(\rho)$. They describe the average contrast in the eigendirections. Thus, the *integration scale* ρ should reflect the characteristic size of the texture. Usually, it is large in comparison to the noise scale σ. The eigenvector w_2 corresponds to the smaller eigenvalue μ_2. It is the orientation with the lowest fluctuations, the so-called *coherence orientation.*

Fig. 1(d) depicts this direction. We observe that it is exactly the desired average orientation. It should also be noted how well the singularities correspond to the singularities in the original fingerprint image.

Not only the eigenvectors, but also the eigenvalues provide useful information. Constant areas are characterized by $\mu_1 = \mu_2 = 0$, straight edges give $\mu_1 \gg \mu_2 = 0$, and corners yield $\mu_1 \geq \mu_2 \gg 0$. The expression

$$\kappa := (\mu_1 - \mu_2)^2 = (j_{11} - j_{22})^2 + 4j_{12}^2 \tag{7}$$

becomes large for anisotropic structures. It measures the *coherence* within a window of scale ρ, and its value can range from 0 to ∞.

The reason why we prefer this coherence measure over the popular *normalized coherence measure*

$$\tilde{\kappa} = \frac{(\mu_1 - \mu_2)^2}{(\mu_1 + \mu_2)^2} = \frac{(j_{11} - j_{22})^2 + 4j_{12}^2}{(j_{11} + j_{22})^2} \tag{8}$$

which attains values between 0 and 1, is that the normalized coherence measure is discontinuous for $\mu_1 = \mu_2 = 0$. This may lead to unreliable coherence estimates in flat image regions. A simple example can illustrate the problem: if $\mu_1 = \mu_2 \downarrow 0$, then $\tilde{\kappa} \to 0$, while $\mu_2 = 0$ and $\mu_1 \downarrow 0$ lead to $\tilde{\kappa} \to 1$. The latter limit also contradicts the intuition that a homogeneous region should reveal no anisotropy.

Now that we have analysed the structure tensor for scalar-valued images, we can draw our attention to the vector-valued case. We denote a vector-valued image by $\vec{u}\ \Omega \to \mathbb{R}^m$and its channels by u_i, $i = 1,\ldots,m$. Di Zenzo [19] proposed an edge detector for vector images by considering the eigenvalues and eigenvectors of

$$\sum_{i=1}^{m} \nabla u_i (\nabla u_i)^T \tag{9}$$

If we extend his idea by introducing a noise and integration scale, this comes down to averaging the structure tensors of

[2] In our terminology, gradients with opposite sign share the same orientation, but point in opposite directions.

each channel in a common structure tensor

$$J_\rho(\nabla \vec{u}_\sigma) = \sum_{i=1}^{m} w_i J_\rho(\nabla u_{i,\sigma}) \tag{10}$$

with $\sum w_i = 1$ and $w_i > 0$ for all i. An interpretation of this structure tensor for vector-valued images in terms of eigenvalues and eigenvectors carries immediately over from the scalar case.

In the absence of specific a priori knowledge or if one has a colour model where all channels have a similar meaning, range and reliability, one usually chooses equal weights:

$$w_i = \frac{1}{m} \quad i = 1, \ldots, m \tag{11}$$

In those cases where measurements in some channels are less reliable or more noisy, one may choose the weights as a function of the noise variance σ_i^2 such that [28]:

$$w_i = \frac{1/\sigma_i^2}{\sum_{j=1}^{m} 1/\sigma_j^2} \quad i = 1, \ldots, m \tag{12}$$

If the noise variance turns out to be signal-dependent, these weights can be adapted locally resulting in an inhomogeneous treatment of the pixels [28].

3. Coherence-enhancing anisotropic diffusion

Now that we have a tool for *analysing* coherence in vector images, we can try to *enhance* it.

This may be achieved by using anisotropic diffusion filtering. In the scalar case the idea is as follows: One obtains a processed version $u(x,t)$ of an image $f(x)$ with a scale parameter $t \geq 0$ as the solution of a diffusion equation

$$\partial_t u = \operatorname{div}(D \nabla u) \tag{13}$$

with f as initial condition,

$$u(x, 0) = f(x) \tag{14}$$

and reflecting boundary conditions:

$$\langle D \nabla u, \vec{n} \rangle = 0 \tag{15}$$

Hereby, $\vec{n}$ denotes the outer normal and $\langle .,. \rangle$ the usual Euclidean scalar product.

The diffusion tensor D is a positive definite 2×2 matrix, which steers the diffusion process: its eigenvalues determine the diffusivities in the directions of the eigenvectors. In the nonlinear case one adapts the diffusion tensor to the evolving image, for instance to reduce undesired smoothing across edges; see [29] and the references therein. The use of a diffusion tensor allows a more flexible, orientation-dependent filter design than early nonlinear diffusion filters [30,31] which use only scalar-valued diffusivities.

The simplest idea to process vector images would be to diffuse each channel separately. If the diffusion tensor depends on the local image structure, however, this causes a risk that a structure (e.g. an edge) evolves at different locations for different channels. Thus, it is plausible to synchronize the evolution by a common diffusion tensor for all channels. In this case the vector-valued diffusion filter has the following structure ($i = 1,\ldots,m$):

$$\partial_t u_i = \operatorname{div}(D \nabla u_i) \tag{16}$$

$$u_i(x, 0) = f_i(x) \tag{17}$$

$$\langle D \nabla u_i, \vec{n} \rangle = 0 \tag{18}$$

Since D should take into account information from all channels, a natural choice would be to make it a function of $J_\rho(\nabla \vec{u}_\sigma)$, the structure tensor for vector images. What should this function look like? For enhancing coherence in vector images, we need a smoothing process which acts mainly along the coherence direction w_2 (with the notations from Section 2) and the smoothing should increase with the coherence $(\mu_1 - \mu_2)^2$. This may be achieved in the following way:

We require that D should possess the same eigenvectors w_1, w_2 as the structure tensor $J_\rho(\nabla \vec{u}_\sigma)$. The eigenvalues of D are chosen as

$$\lambda_1 := \alpha \tag{19}$$

$$\lambda_2 := \begin{cases} \alpha & \text{if } \mu_1 = \mu_2, \\ \alpha + (1-\alpha) \exp\left(\dfrac{-C}{(\mu_1 - \mu_2)^2} \right) & \text{else} \end{cases} \tag{20}$$

with $C > 0$ and a small parameter $\alpha \in (0,1)$.

We observe that λ_2 is an increasing function with respect to the coherence $(\mu_1 - \mu_2)^2$. Since the corresponding eigenvector w_2 describes the coherence direction, we have constructed a diffusion process acting preferably along coherent structures.

The exponential function and the positive parameter α were introduced mainly for two theoretical reasons: First, the exponential function guarantees that the smoothness of the structure tensor carries over to the diffusion tensor, and that λ_2 does not exceed 1. This bound is a typical scaling convention in nonlinear diffusion filtering. Second, the positivity of α guarantees that the process never stops: Even if the structure becomes isotropic ($(\mu_1 - \mu_2)^2 \to 0$), there remains some small linear diffusion with diffusivity $\alpha > 0$. Thus, the diffusion tensor is uniformly positive definite.

Exploiting the smoothness and uniform positive definiteness properties, we may find a well-founded scale-space interpretation in a similar way as for the scalar-valued anisotropic diffusion filters from [2]. This scale-space representation simplifies the vector image with respect to many aspects: within each channel maxima decrease, minima increase, all L^p-norms ($2 \leq p \leq \infty$) decrease, even central moments are diminished, and the entropy increases. Moreover, the solution depends continuously on the original image. For $t \to \infty$, all channels tend to a constant image.

The average value within each channel remains unaltered during the whole evolution. Existence and uniqueness results for this initial boundary value problem can be obtained in a similar way as in [31]. For a more detailed treatment of the well-posedness and scale-space theory for scalar-valued anisotropic diffusion filters in the continuous and discrete setting, the reader is referred to [29].

4. Parameter selection

The preceding model contains several parameters which have to be specified in practical situations. The goal of this section is to clarify their meaning and to present empirical guidelines for their selection.

We have already seen that the regularization parameter α was introduced to ensure a small amount of isotropic diffusion and to limit the spectral condition number of the diffusion tensor to $1/\alpha$. This parameter is mainly important for theoretical reasons. In practice, it can be fixed to a small value, and no adaptation to the actual image material is required.

The parameter C is a threshold parameter. Structures with coherence measures $(\mu_1 - \mu_2)^2 \ll C$ are regarded as almost isotropic, and the diffusion along the coherence direction w_2 tends to α. For $(\mu_1 - \mu_2)^2 \gg C$, the diffusion along the coherence direction w_2 tends to its maximal value, which is limited by 1. One possibility to determine a good practical value for C is to calculate a cumulate histogram for $(\mu_1 - \mu_2)^2$ evaluated for the initial image f, and to set C to a certain quantile of this histogram. For instance, if one estimates that 95% of the image locations have strongly preferred one-dimensional structures, one may set C to the 95% quantile of the process.

Since the time t is an inherent parameter in each continuous diffusion process, it has nothing to do with its discretization. The common tradition in image analysis, however, is to assign unit length to a pixel. In this case, a different discretization has to be regarded as a rescaling of the image domain. The scaling behaviour of diffusion processes implies that a spatial rescaling which replaces x by βx, has to replace t by $\beta^2 t$. This means for instance that a subsampling in each image direction by a factor 2 results in a four times faster image evolution. Moreover, typical finite difference implementations reveal a computational effort which is proportional to the pixel number. This gives another speed-up by a factor 4, such that the whole calculation becomes 16 times faster.

There remains another question to be addressed: what is a suitable stopping time t of the process?[3] Let us first address this question for scalar-valued images. In a classic linear scale-space representation based on the diffusion process $\partial_t u = \Delta u$, the time t corresponds to a convolution with a Gaussian of standard deviation $\sigma = \sqrt{2t}$. Thus, specifying a spatial smoothing radius σ immediately determines the stopping time t.

In the nonlinear diffusion case, the smoothing is nonuniform and the time t is not directly related to a spatial scale. Other intuitive measures like counting the number of extrema are also problematic for diffusion filters, since it is well known that for linear and nonlinear diffusion filters in dimensions ≥ 2, the number of local extrema does not necessarily decrease in a monotone way: creation of extrema is not an exception but an event which happens generically [32].

However, it is possible to define average measures for the globality of the representation which reveal monotone behaviour. By identifying it as a Lyapunov functional of a large class of scalar-valued nonlinear diffusion filters, Weickert [2,29] has shown that the variance $\eta^2(u(t))$ is monotonously decreasing. This reasoning immediately carries over to vector-valued images, where one may define the variance as a suitable convex combination of the variances in each channel:

$$\eta^2(\vec{u}(t)) = \sum_{i=1}^{m} \beta_i \eta^2(\vec{u}_i(t)) \tag{21}$$

with $\Sigma_i \beta_i = 1$ and $\beta_i > 0$ for all i. We also know that $\eta^2(\vec{u}(\infty)) = 0$, since every channel converges to a constant image. Therefore, the relative variance

$$s_{\vec{f}}(\vec{u}(t)) = \frac{\eta^2(\vec{u}(t))}{\eta^2(\vec{f})} \tag{22}$$

decreases monotonically from 1 to 0. It gives the average locality of $\vec{u}(t)$ and its value can be used to measure the distance of $\vec{u}(t)$ from the initial state $\vec{f}$ and the final state $\vec{u}(\infty)$. Prescribing a certain value for $s_{\vec{f}}$ provides us with an a posteriori criterion for the stopping time of the nonlinear diffusion process. Moreover, this strategy frees the users from any recalculations of the stopping time, if the image is resampled. Practical applications to the restoration of scalar valued medical images have demonstrated the usefulness and simplicity of this criterion [33,34].

The relative variance can also be used as a heuristic guideline for restoring images with a known signal-to-noise ratio (SNR). Let us illustrate this for a simple example where a degraded image $\vec{g}$ is a noisy variant of some original image $\vec{f}$. By defining the SNR as the ratio between the variance of the original image and the noise variance, one knows that

$$\frac{\eta^2(\vec{f})}{\eta^2(\vec{g})} = \frac{1}{1 + \frac{1}{\mathrm{SNR}}} \tag{23}$$

An ideal diffusion filter which works optimally for a denoising task would first eliminate the noise before significantly affecting the signal. For such a filter, one should choose the

[3] It should be observed that this question only appears when regarding the diffusion process as a *restoration method*. Considering it as a *scale-space* means that one is interested in the entire evolution.

stopping time T such that the relative variance satisfies

$$s_{\vec{g}}(\vec{u}(T)) = \frac{1}{1+\frac{1}{\mathrm{SNR}}} \tag{24}$$

This stopping time is uniquely determined, as we know that $s_{\vec{g}}(\vec{u}(t))$ is monotone in t. In practice, such a stopping criterion may underestimate the optimal stopping time, since even a well-adapted diffusion filter cannot completely avoid influencing the signal to a certain amount while eliminating the noise. Nevertheless, in Section 5 we shall see that Eq. (24) can give results which are rather close to the optimal value.

The local scale σ and the integration scale ρ of the

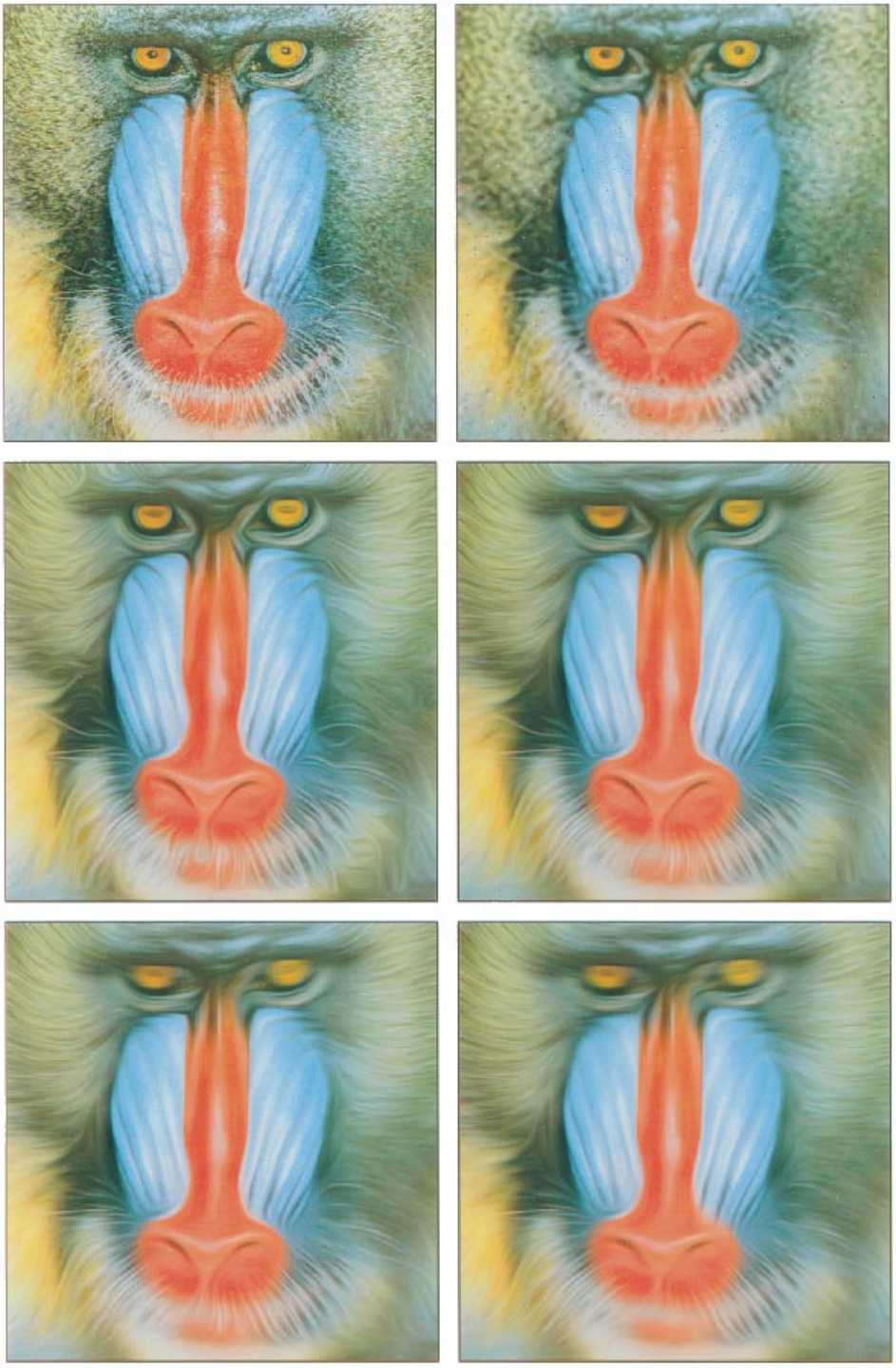

Fig. 2. Coherence-enhancing diffusion of the mandrill test image with different integration scales ρ. C was set to the 99% quantile. (a) Top left: Original, $\Omega = (0,512)^2$. (b) Top right: Filtered with $\sigma = 1$, $\rho = 0$, $t = 40$ (c) Middle left: Ditto with $\rho = 5$. (d) Middle right: $\rho = 10$. (e) Bottom left: $\rho = 15$. (f) Bottom right: $\rho = 20$.

structure tensor should be adapted to the noise and the texture scale of the problem. In many cases it is not very difficult to get parameter estimates which work well over the whole image domain. In other situations, one may want to find local estimates by applying scale selection strategies as proposed by Lindeberg [25]. The next section will show an example which illustrates the impact of the integration scale.

5. Examples

Coherence-enhancing anisotropic diffusion can be implemented by means of standard finite-difference methods from the numerical literature; see [35] for some implementational details as well as extensions to higher dimensions. In the following test examples we used the RGB channels to

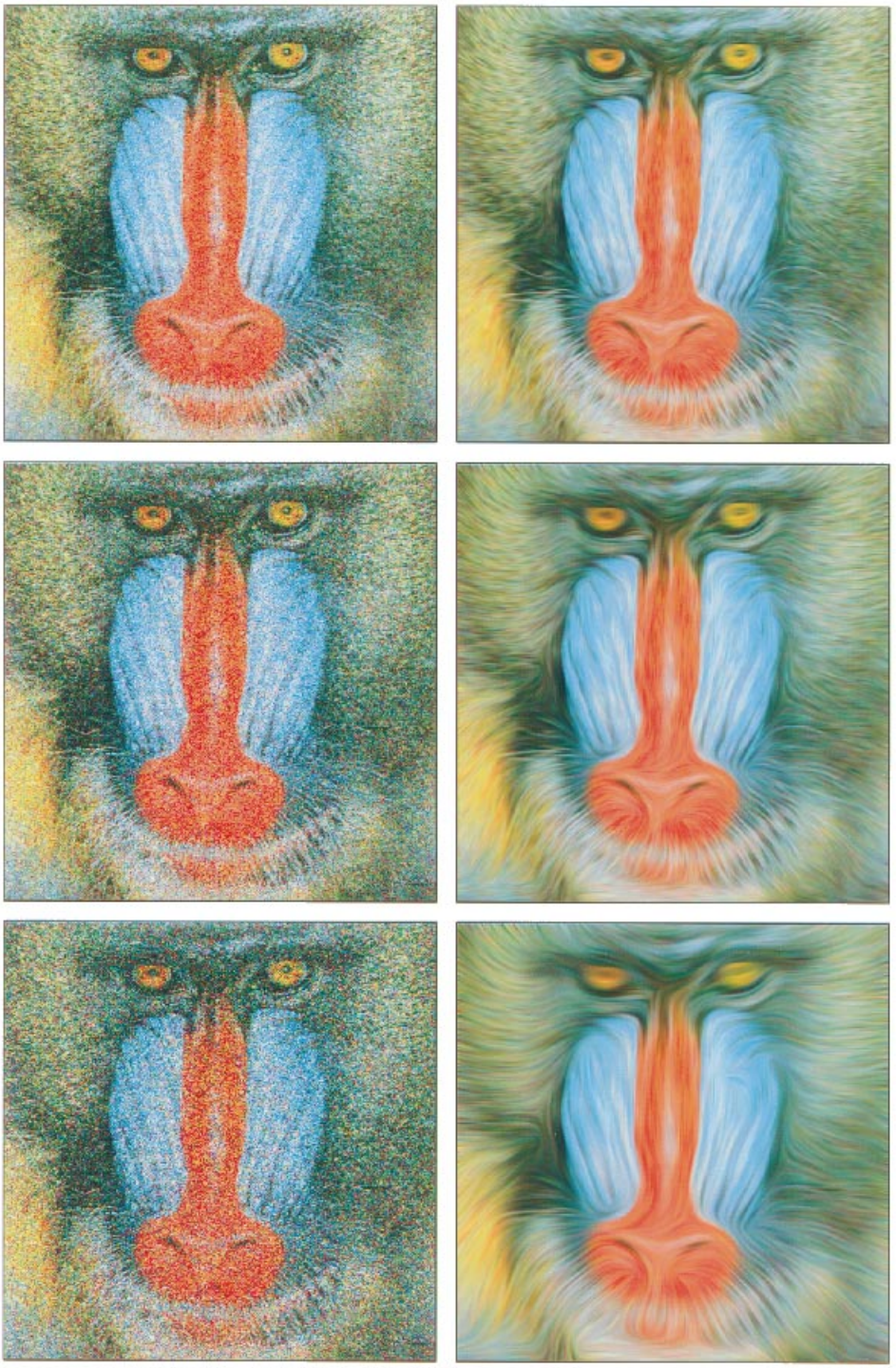

Fig. 3. Robustness of coherence-enhancing diffusion under noise ($\sigma = 1$, $\rho = 12$, λ was set to the 99% quantile). (a) Top left: Mandrill image with additive Gaussian noise. $\eta_n = 56.2$, SNR $= 1$. (b) Top right: Optimal restoration of (a); $t = 6.4$. (c) Middle left: $\sigma_n = 79.0$, SNR $= 0.5$. (d) Middle right: Optimal restoration of (c); $t = 16.5$. (e) Bottom left: $\sigma_n = 112.4$, SNR $= 0.25$. (f) Bottom right: Optimal restoration of (e); $t = 46.0$.

Table 1
Restoration properties of coherence-enhancing diffusion applied to the mandrill image with additive Gaussian noise with zero mean

	SNR				
	4	2	1.0	0.5	0.25
η_n	28.1	39.7	56.2	79.0	112.4
T	1.3	2.7	6.4	16.5	46.0
$\eta^2\ (t=0)$	3945.34	4730.24	6308.89	9384.54	15761.21
$\eta^2\ (t=T)$	2990.08	2917.97	2807.48	2669.16	2502.25
$\delta\ (t=0)$	787.50	1571.88	3149.99	6224.20	12599.97
$\delta\ (t=T)$	299.13	415.21	547.20	678.24	808.29
$\delta(0)/\delta(T)$	2.63	3.79	5.76	9.18	15.58

η_n denotes the standard deviation of the noise, and η^2 is the average image variance per channel. T is the optimal stopping time with respect to the minimization of $\delta(t)$, the l^2 distance between $\vec{u}(t)$ and the uncorrupted original image.

Table 2
Restoration properties of coherence-enhancing diffusion when applying the stopping time criterion instead of the optimal stopping time

	SNR				
	4	2	1.0	0.5	0.25
η_n	28.1	39.7	56.2	79.0	112.4
T	0.7	1.3	2.4	4.8	9.0
$\eta^2\ (t=0)$	3945.34	4730.24	6308.89	9384.54	15761.21
$\eta^2\ (t=T)$	3155.85	3144.92	3143.47	3119.03	3145.70
$\delta\ (t=0)$	787.50	1571.88	3149.99	6224.20	12599.97
$\delta\ (t=T)$	299.13	415.21	547.20	678.24	808.29
$\delta(0)/\delta(T)$	2.46	3.48	5.14	7.93	12.55

regard colour images as vector images. Since the variances in all channels were comparable and no additional a priori knowledge was available, equal weights were assigned to all channels. The parameter α was set to 0.001.

Fig. 2 shows the well-known mandrill test image and its processed version for different integration scales ρ. The case $\rho = 0$ is depicted in Fig. 2(b). This choice is essentially a colour extension of the greyscale model by Cottet and Germain [11], and its smoothing direction w_2 is identical with the Chambolle and Sapiro-Ringach filters [6,9]. As can be seen from Fig. 1(b), the reason for the limited performance of this filter in the context of orientation smoothing lies in highly fluctuating local orientation estimates. The introduction of an additional integration scale stabilizes these estimates and leads to a significantly improved smoothing along coherent structures such as the mandrill's hair. This effect, depicted in Fig. 2(c–f), shows that *the integration scale is an important feature for the success of any orientation diffusion scheme*. It should be equal to or larger than the texture scale. Overestimating it is significantly less critical than underestimations.

Fig. 3 analyses the behaviour of coherence-enhancing

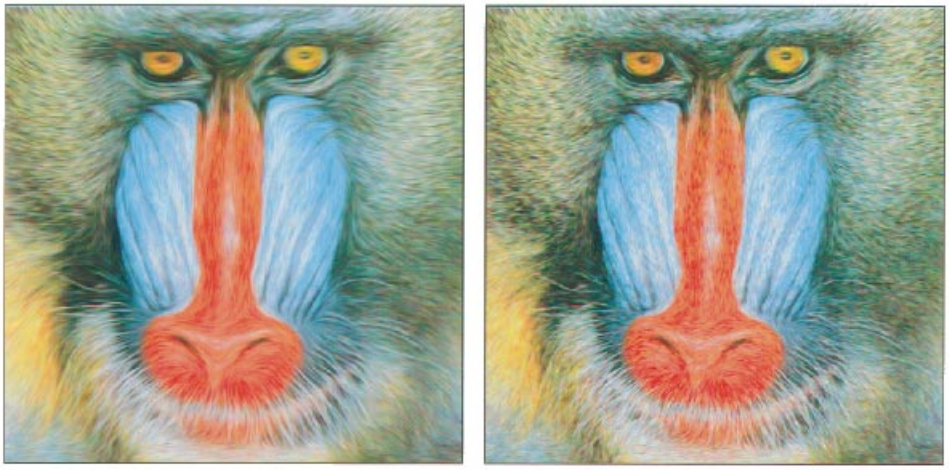

Fig. 4. Optimal stopping time vs. automatic stopping time. (a) Left: Optimal restoration of mandrill image with additive Gaussian noise (SNR = 1). (b) Right: Restoration according to the stopping criterion (Eq. (24)).

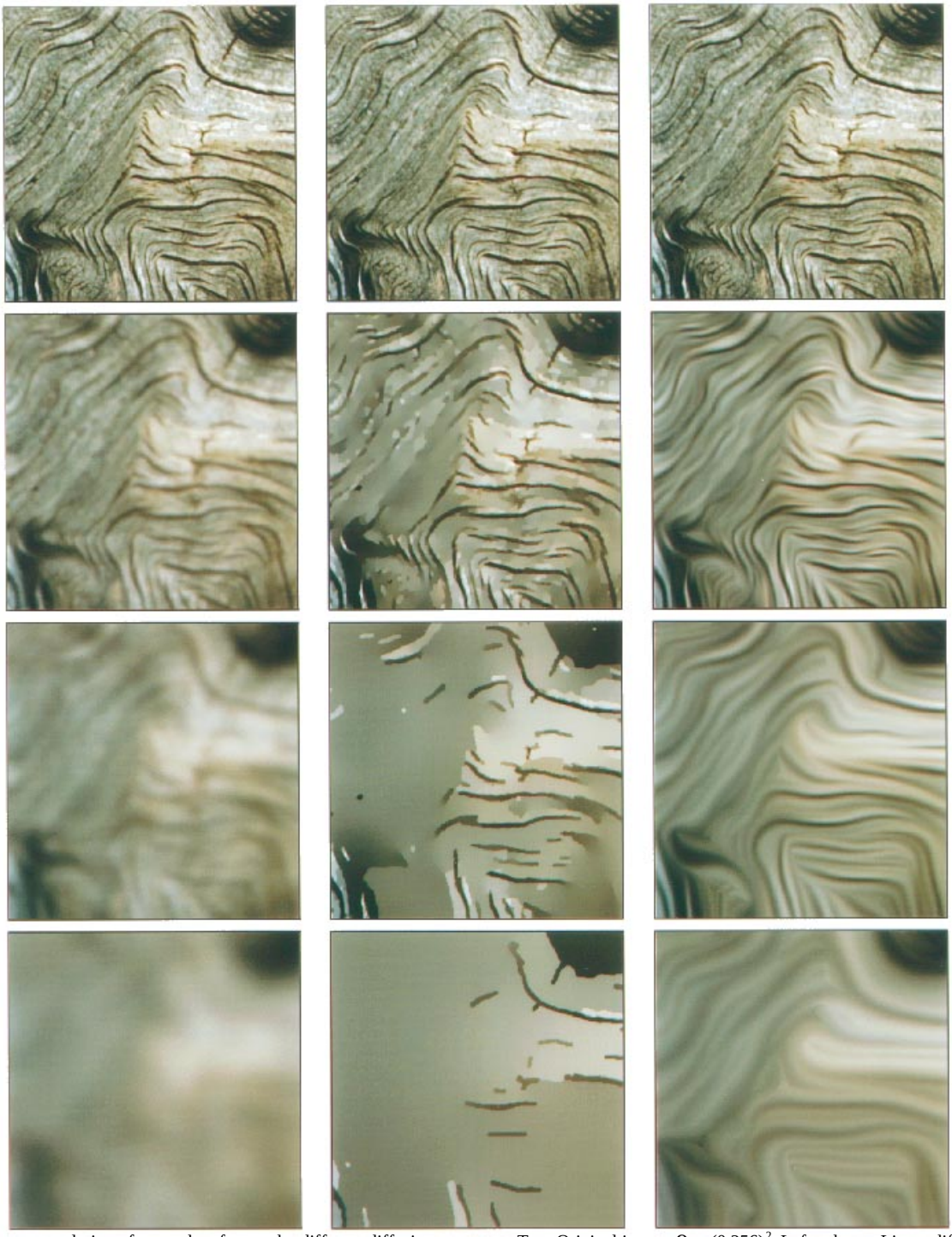

Fig. 5. Scale-space evolution of a wood surface under different diffusion processes. Top: Original image, $\Omega = (0,256)^2$. Left column: Linear diffusion, top to bottom: $t = 0$, 2, 10, 50. Middle column: Isotropic nonlinear diffusion ($\lambda = 10$, $\sigma = 1$), $t = 0$, 20, 200, 2000. Right column: Coherence-enhancing nonlinear diffusion ($C = 17.6$, $\sigma = 1$, $\rho = 5$), $t = 0$, 20, 200, 2000.

diffusion for noisy input images. The mandrill image has been corrupted with additive Gaussian noise and the filtered results were depicted at those times when the l^2 distance to the uncorrupted mandrill image was minimal. The observable high robustness confirms the theoretically established stability of a broad class of nonlinear diffusion filters under perturbations of the original image [29]. Even for a SNR of only 0.25 and a noise scale of only $\sigma = 1$ pixel, it is possible to correctly restore many coherent structures which are hardly visible for a human observer. Table 1 shows that in this case coherence-enhancing diffusion was able to reduce the l^2 distance to the original image by a factor 15.58. Table 2 and Fig. 4 illustrate the denoising behaviour when using the stopping criterion (Eq. (24)). We observe that the

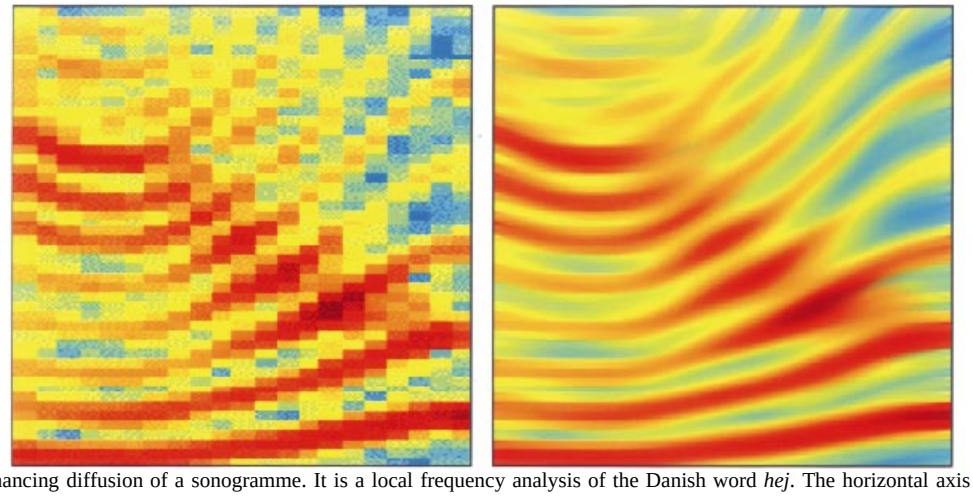

Fig. 6. Coherence-enhancing diffusion of a sonogramme. It is a local frequency analysis of the Danish word *hej*. The horizontal axis is the time axis, the vertical axis describes the logarithm of the frequency, and the colours display their intensities. One is interested in estimating the distance between the different lines, and in interpolating such that sampling artefacts become smaller. (a) Left: $\Omega = (0,168) \times (0,192)$. (b) Right: Filtered ($C = 28.5$ (99% quantile), $\sigma = 1$, $\rho = 10$, $t = 50$).

improvements in the l^2 distance are not much worse than in the optimal case.

After these discussions on the restoration properties of coherence-enhancing diffusion, let us now have a look at its scale-space qualities. Fig. 5 depicts the evolution of a wood surface under three diffusion scale-spaces. The first column shows the results when isotropic linear diffusion with the unit matrix as diffusion tensor is applied. Since this scale-space is designed to be uncommitted, it blurs all features in a uniform way. In the middle column evolution under nonlinear isotropic diffusion filtering can be seen. This method is based on an extension of the techniques from [30,31] to vector images; see [4] for more details. It can be regarded as an edge-preserving smoothing where the (scalar-valued) diffusivity is low whenever $\Sigma_i |\nabla u_{i,\sigma}|^2$ is large. It tends to preserve high contrasts, but it is ignorant of the flow-like image character. The right column shows the effect of coherence-enhancing anisotropic diffusion. We observe that it gives a flow-like gradual simplification of the original image. It is our belief that an evolution of this type will be potentially useful for the automatic grading of wood surfaces. This would be in accordance with the good results of coherence-enhancing diffusion filtering for the grading of scalar-valued nonwoven fabric images that were reported in [3].

Other potential application fields where one might be interested in processing coherent structures are sketched in Figs 6 and 7. They describe problems from analysing

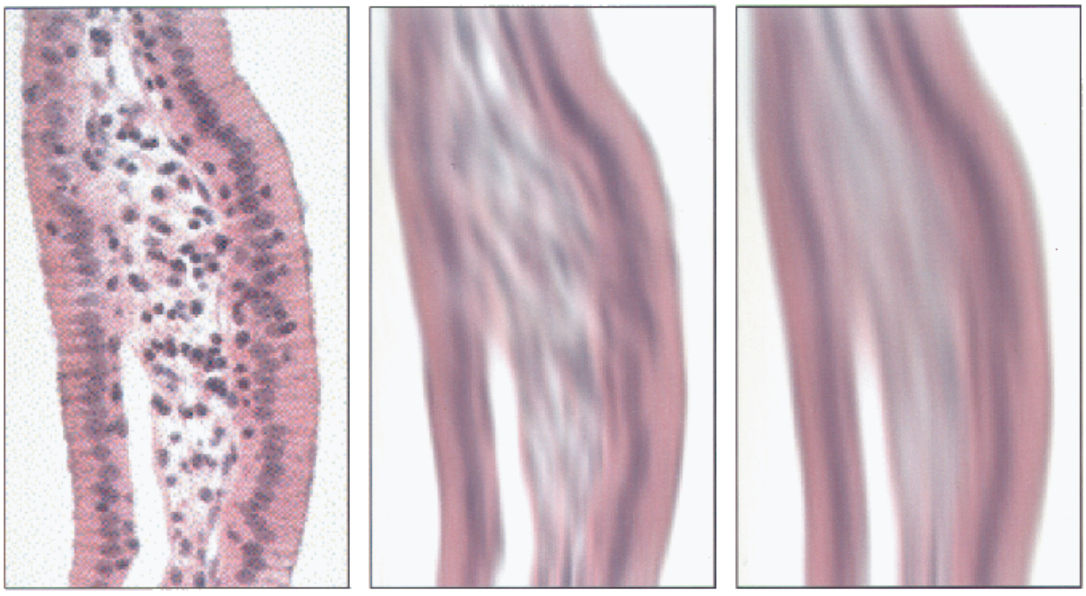

Fig. 7. Coherence-enhancing colour diffusion for simplifying medical images. This is of potential interest for easing their automatic evaluation by subsequent image processing methods. (a) Left: Light microscopy image of a columnar epithelium of the gall bladder, $\Omega = (0,125) \times (0,212)$. (b) Middle: Filtered ($\sigma = 1$, $\rho = 30$, $C = 1$, $t = 30$). (c) Ditto with $t = 100$.

Fig. 8. Coherence-enhancing anisotropic diffusion of an expressionistic painting ($C = 4.6$ (99% quantile), $\sigma = 1$, $\rho = 4$). (a) Top left: 'Starry Night' by van Gogh (Saint-Rémy, 1889; The Museum of Modern Art, New York), $\Omega = (0,500) \times (0,406)$. (b) Top right: $t = 15$. (c) Bottom left: $t = 300$. (d) Bottom right: $t = 3000$.

sonogrammes and medical images from light microscopy, respectively.

Since coherence-enhancing anisotropic colour diffusion seems to create optically pleasant structures, it is tempting to apply it to van Gogh paintings which emphasize such coherent structures. Thus, in a last example the temporal evolution of the 'Starry Night' painting is shown in Fig. 8 [36]. While the image becomes gradually simpler, its flow-like character, which is typical for many van Gogh paintings, is maintained for a very long time. The coherence-enhancing effect even creates full moon.

6. Conclusions

In this paper a filter for enhancing coherent structures in vector-valued images has been presented. It is based on two ideas: a generalized structure tensor for vector images, and anisotropic nonlinear diffusion filtering with a diffusion tensor. We have shown that its main distinction from other colour diffusion models lies in an additional integration scale which gives a semilocal average over the preferred orientation. This integration leads to significantly improved smoothing orientations, which is of importance for the enhancement of one-dimensional structures. We have clarified the role of the necessary parameters and proposed heuristics for their selection. Examples have been presented which show that coherence-enhancing colour diffusion is very robust under noise and of potential interest in various application areas.

Acknowledgements

This work has been funded by *Stiftung Innovation des Landes Rheinland-Pfalz*, the *Real World Computing Partnership*, the *Danish National Science Research Council*, and the *EU-TMR project VIRGO*. The sonogramme has been provided by Kristoffer Jensen.

References

[1] B. Jähne, Spatio-temporal image processing, Lecture Notes in Comp. Science, Vol. 751, Springer, Berlin, 1993.

[2] J. Weickert, Scale-space properties of nonlinear diffusion filtering with a diffusion tensor, Report No. 110, Laboratory of Technomathematics, University of Kaiserslautern, P.O. Box 3049, 67653 Kaiserslautern, Germany, 1994.
[3] J. Weickert, Multiscale texture enhancement, in: V. Hlaváč, R. Šára (Eds.), Computer Analysis of Images and Patterns, Lecture Notes in Comp. Science, Vol. 970, Springer, Berlin, 1995, pp. 230–237.
[4] R. Whitaker, G. Gerig, Vector-valued diffusion, in: B.M. ter Haar Romeny (Ed.), Geometry-driven Diffusion in Computer Vision, Kluwer, Dordrecht, 1994, pp. 93–134.
[5] P. Blomgren, T.F. Chan, Color TV: total variation methods for restoration of vector valued images, IEEE Trans. Image Proc. 7 (1998) 304–309.
[6] A. Chambolle, Partial differential equations and image processing, in: Proc. IEEE Int. Conf. Image Processing (ICIP-94, Austin, Nov. 13–16, 1994), Vol. 1, IEEE Computer Society Press, Los Alamitos, 1994, pp. 16–20.
[7] R. Kimmel, N. Sochen, R. Malladi, Images as embedding maps and minimal surfaces: Movies, color, and volumetric medical images, in: Proc. IEEE Comp. Soc. Conf. Computer Vision and Pattern Recognition (CVPR '97, San Juan, June 17–19, 1997), IEEE Computer Society Press, Los Alamitos, 1997, pp. 350–355.
[8] M. Proesmans, E.J. Pauwels, L.J. Van Gool, Coupled geometry-driven diffusion equations for low-level vision, in: B.M. ter Haar Romeny (Ed.), Geometry-driven Diffusion in Computer Vision, Kluwer, Dordrecht, 1994, pp. 191–228.
[9] G. Sapiro, D.L. Ringach, Anisotropic diffusion of multivalued images with applications to color filtering, IEEE Trans. Image Proc. 5 (1996) 1582–1586.
[10] J. Shah, Curve evolution and segmentation functionals: application to color images, in: Proc. IEEE Int. Conf. Image Processing (ICIP-96, Lausanne, Sept. 16–19, 1996), Vol. 1, 1996, pp. 461–464.
[11] G.-H. Cottet, L. Germain, Image processing through reaction combined with nonlinear diffusion, Math. Comp. 61 (1993) 659–673.
[12] M. Nitzberg, T. Shiota, Nonlinear image filtering with edge and corner enhancement, IEEE Trans. Pattern Anal. Mach. Intell. 14 (1992) 826–833.
[13] T. Lindeberg, J. Gårding, Shape-adapted smoothing in estimation of 3-D depth cues from affine distortions of local 2-D brightness structure, Image Vision Comput. 15 (1997) 415–434.
[14] G.Z. Yang, P. Burger, D.N. Firmin, S.R. Underwood, Structure adaptive anisotropic filtering, Image Vision Comput. 14 (1996) 135–145.
[15] J. Weickert, Theoretical foundations of anisotropic diffusion in image processing, Computing (Suppl. 11) (1996) 221–236.
[16] Y. Rubner, C. Tomasi, Coalescing texture descriptors, in: Proc. ARPA Image Understanding Workshop, Palm Springs, February 1996, 1996, pp. 927–936.
[17] R. Carmona, S. Zhong, Adaptive smoothing respecting feature directions, IEEE Trans. Image Proc. 7 (1998) 353–358.
[18] E. Kreyszig, Differential Geometry, University of Toronto Press, Toronto, 1959.
[19] S. Di Zenzo, A note on the gradient of a multi-image, Computer Vision, Graphics, and Image Processing 33 (1986) 116–125.
[20] B. Cabral, L. Leedom, Imaging vector fields using line integral convolution, Computer Graphics 27 (4) (1993) 263–272.
[21] J. Weickert, Coherence-enhancing diffusion of colour images, in: A. Sanfeliu, J.J. Villanueva, J. Vitrià (Eds.), Proc. VII National Symposium on Pattern Recognition and Image Analysis (VII NSPRIA, Barcelona, April 21–25, 1997), Vol. 1, 1997, pp. 239–244.
[22] A.R. Rao, B.G. Schunck, Computing oriented texture fields, CVGIP: Graphical Models and Image Processing 53 (1991) 157–185.
[23] M.A. Förstner, E. Gülch, A fast operator for detection and precise location of distinct points, corners and centres of circular features, in: Proc. ISPRS Intercommission Conf. on Fast Processing of Photogrammetric Data, Interlaken, 1987, pp. 281–305.
[24] C.G. Harris, M. Stephens, A combined corner and edge detector, in: Proc. Fourth Alvey Vision Conf. (AVC 88, Manchester, Aug. 31–Sept. 2, 1988), 1988, pp. 147–152.
[25] T. Lindeberg, Scale-space Theory in Computer Vision, Kluwer, Boston, 1994.
[26] M. Kass, A. Witkin, Analyzing oriented patterns, Computer Vision, Graphics, and Image Processing 37 (1987) 362–385.
[27] J. Bigün, G.H. Granlund, Optimal orientation detection of linear symmetry, in: Proc. First Int. Conf. on Computer Vision (ICCV '87, London, June 8–11, 1987), IEEE Computer Society Press, Washington, 1987, pp. 433–438.
[28] R. Brügelmann, W. Förstner, Noise estimation for color edge extraction, in: W. Förstner, S. Ruwiedel (Eds.), Robust Computer Vision, Wichmann, Karlsruhe, 1992, pp. 90–107.
[29] J. Weickert, Anisotropic Diffusion in Image Processing, Teubner, Stuttgart, 1998.
[30] P. Perona, J. Malik, Scale space and edge detection using anisotropic diffusion, IEEE Trans. Pattern Anal. Mach. Intell. 12 (1990) 629–639.
[31] F. Catté, P.-L. Lions, J.-M. Morel, T. Coll, Image selective smoothing and edge detection by nonlinear diffusion, SIAM J. Numer. Anal. 29 (1992) 182–193.
[32] J.H. Rieger, Generic evolution of edges on families of diffused grey-value surfaces, J. Math. Imag. Vision 5 (1995) 207–217.
[33] J. Weickert, K.J. Zuiderveld, B.M. ter Haar Romeny, W.J. Niessen, Parallel implementations of AOS schemes: A fast way of nonlinear diffusion filtering, in: Proc. 1997 IEEE International Conference on Image Processing (ICIP-97, Santa Barbara, Oct. 26–29, 1997), Vol. 3, 1997, pp. 396–399.
[34] W.J. Niessen, K.L. Vincken, J. Weickert, M.A. Viergever, Three-dimensional MR brain segmentation, in: Proc. Sixth Int. Conf. on Computer Vision (ICCV '98, Bombay, Jan. 4–7, 1998), 1998, pp. 53–58.
[35] J. Weickert, B.M. ter Haar Romeny, A. Lopez, W.J. van Enk, Orientation analysis by coherence-enhancing diffusion, in: Proc. Symp. Real World Computing (RWC '97, Tokyo, Jan. 29–31, 1997), 1997, pp. 96–103.
[36] V. van Gogh, Starry night, Saint-Rémy, 1889. The Museum of Modern Art, New York.